



HAL
open science

Effect of mechanical boundary conditions on the flow reversal in square Rayleigh-Bénard cells.

Andrés Castillo-Castellanos, Anne Sergent, Maurice Rossi

► To cite this version:

Andrés Castillo-Castellanos, Anne Sergent, Maurice Rossi. Effect of mechanical boundary conditions on the flow reversal in square Rayleigh-Bénard cells.. 18ème Rencontre du Non-Linéaire, Université Paris Diderot - Paris 7, Mar 2015, Paris, France. pp.ISBN: 978-2-9538596-4-5. hal-01429811

HAL Id: hal-01429811

<https://hal.sorbonne-universite.fr/hal-01429811>

Submitted on 9 Jan 2017

HAL is a multi-disciplinary open access archive for the deposit and dissemination of scientific research documents, whether they are published or not. The documents may come from teaching and research institutions in France or abroad, or from public or private research centers.

L'archive ouverte pluridisciplinaire **HAL**, est destinée au dépôt et à la diffusion de documents scientifiques de niveau recherche, publiés ou non, émanant des établissements d'enseignement et de recherche français ou étrangers, des laboratoires publics ou privés.

Effect of mechanical boundary conditions on the flow reversal in square Rayleigh-Bénard cells.

Andrés Castillo-Castellanos^{1,2,3}, Anne Sergent^{2,3} & Maurice Rossi^{1,3}

¹ Institut ∂ Alembert, 4 Place Jussieu, Paris, 75252 CEDEX 05, France.

² LIMSI-CNRS, rue John von Neuman, Orsay, 91403 CEDEX, France.

³ Université Pierre et Marie Curie - Paris 6, 4 Place Jussieu, Paris, 75252 CEDEX 05, France.

`andres.castillo@dalembert.upmc.fr`

Résumé. On étudie l'influence des conditions mécaniques imposées aux bords sur les renversements observés dans une cellule de convection de Rayleigh-Bénard de forme carrée. On considère deux configurations avec des conditions mécaniques différentes sur la plaque supérieure : i) condition de non-glissement comme dans le cas classique (RBC), et ii) condition de glissement (RBS). Les nombres de Rayleigh et Prandtl utilisés sont tels qu'on observe des renversements dans les deux cas. Le mécanisme de renversement est le même pour les deux configurations. Toutefois les renversements sont plus courts et plus fréquents pour RBS que pour RBC. La température moyenne est significativement plus basse et le flux de chaleur plus élevé pour RBS. Au cours d'un processus de renversement, on effectue un bilan énergétique et on suit l'évolution de l'énergie potentielle disponible. Le flux de chaleur entrant dans le système est converti en énergie potentielle disponible qui s'accumule à l'intérieur des écoulements de coin contra-rotatifs ainsi que dans la couche limite thermique, conduisant ainsi à une augmentation de volume de ces écoulements de coin.

Abstract. This study explores the effects of mechanical boundary conditions on flow reversals observed inside square Rayleigh-Bénard convection cells. We consider two configurations where different conditions are imposed on the top boundary: i) a no-slip condition as in the classical case (RBC) and ii) a free-slip condition (RBS). The *Rayleigh* and *Prandtl* numbers are fixed to values where flow reversals are observed for both configurations. The reversal mechanism is the same for both cases. However reversals are shorter and more frequent for RBS than RBC. The bulk temperature is revealed to be significantly lower and the heat flux larger for RBS. During a standard reversal process, we perform a mechanical energy budget and follow the evolution of the available potential energy. Heat entering the system is transformed into available potential energy and accumulates inside counter-rotating corner flows and thermal boundary layers, prompting corner flows to grow.

1 Introduction

Forced two-dimensional turbulence in the presence of rigid boundaries is characterized by self-organization into coherent structures heavily dependent on the domain geometry. For a square domain, a spontaneous *spin-up* is observed [1] with a single central vortex and small counter-rotating corner flows. In semi-regular intervals, this structure breaks and subsequently reorganizes itself into a new central vortex. In the classical Rayleigh-Bénard (RB) convection problem, this behavior has been observed numerically [2, 3] and experimentally [3]. The flow reversal mechanism is identified in Ref. [2] using Fourier analysis. One obtains dominating modes corresponding to single roll, double rolls and four rolls flow configurations. Flow reversal is described as the transition between these different modes *via* the corner flows. More recently, proper orthogonal decomposition analysis was used [4] to extract coherent structures naturally associated with the flow. This approach which is more adequate, gave results consistent with those of Ref. [2].

The boundary conditions (BC) influence on the dynamics of two-dimensional convection cells has been recently explored [5]: it was observed that mechanical boundary conditions have a larger impact on the system than thermal conditions. In the present paper, we study the influence of mechanical boundary conditions on flow reversals inside square RB cells. We consider two RB cells where only the top BC are changed: i) a no-slip condition as in the classical case (RBC), and ii) a free-slip condition (RBS).

2 Problem setting

2.1 Model equations

Let us consider a fluid contained in a square domain $[-H/2, H/2] \times [-H/2, H/2]$ with adiabatic no-slip sidewalls and a constant temperature T_{bot} (resp. T_{top}) imposed at the bottom (resp. the top). The *Rayleigh* and *Prandtl* numbers are defined as

$$\text{Ra} \equiv \frac{g\beta H^3 [\Theta]}{\kappa\nu} \quad \text{Pr} \equiv \frac{\nu}{\kappa} \quad (1)$$

where g is gravity, β volumetric thermal expansion coefficient, κ fluid thermal diffusivity, ν kinematic viscosity and $[\Theta] = T_{\text{bot}} - T_{\text{top}} > 0$. The characteristic length and velocity used to obtain the dimensionless system of equations are the height H and $\frac{\kappa}{H}\sqrt{\text{Ra}}$, respectively. $\mathbf{x} = (x, z)$ is the coordinate vector, where x and z stand for the horizontal and vertical directions. The dimensionless velocity $\mathbf{u} = (u, w)$ and reduced temperature θ then satisfy the dimensionless Boussinesq equations

$$\begin{cases} \nabla \cdot \mathbf{u} = 0, \\ \partial_t \mathbf{u} + \nabla \cdot [\mathbf{u} \otimes \mathbf{u}] = -\nabla p + \text{Pr Ra}^{-\frac{1}{2}} \Delta \mathbf{u} + \text{Pr} \theta \mathbf{e}_z, \\ \partial_t \theta + \nabla \cdot [\mathbf{u} \theta] = \text{Ra}^{-\frac{1}{2}} \Delta \theta. \end{cases} \quad (2)$$

Sidewalls are adiabatic. On top (resp. bottom) walls, a temperature $\theta = -0.5$ (resp. $\theta = 0.5$) is imposed. For velocity no-slip conditions $\mathbf{u} = 0$ are imposed on the side and bottom walls. For the top boundary either a no-slip condition $u = w = 0$ (RBC), or a free-slip condition, $\partial_z u = w = 0$ (RBS) is imposed.

The values of $\text{Ra} - \text{Pr}$ used for direct numerical simulations (DNS) correspond to a turbulent flow regime, where reversals have been reported [2, 3]: $\text{Pr} = 4.3$ (value for water at 40 °C) and from $\text{Ra} = 10^7$ to 5×10^7 . In the following, for any field $A(\mathbf{x}, t)$, $\langle A \rangle$ (resp. \bar{A}) stands for spatial (resp. temporal) average.

2.2 Numerical method and spatial resolution

The model equations (eq. 2) are discretized using Bell-Colella-Glaz advection scheme [6], [7]. Solutions are obtained for more than 8,000 convective time units. Spatial resolution requirements for DNS [8] are verified using the Nusselt number $\bar{\text{Nu}} = \sqrt{\text{Ra}} \langle w \theta \rangle - \langle \partial_z \theta \rangle$. For RBC [9], as well as for RBS, exact equalities can be written for the time-averaged Nusselt number $\bar{\text{Nu}}$ and the thermal dissipation rate $\bar{\text{Nu}}_\theta \equiv \langle \nabla \theta \cdot \nabla \theta \rangle_V$ or the viscous dissipation rate $\bar{\text{Nu}}_\epsilon \equiv \langle \nabla \mathbf{u} : \nabla \mathbf{u} \rangle_V + 1$. Lack of numerical convergence of $\bar{\text{Nu}}_\theta$ and $\bar{\text{Nu}}_\epsilon$ with the time-averaged Nusselt averaged over the top plate $\bar{\text{Nu}}_{\text{top}}$ and bottom plate $\bar{\text{Nu}}_{\text{bot}}$ could indicate that spatial resolution is insufficient. For two values of $\text{Ra} - \text{Pr}$, these Nusselt values converge within 1% when evaluated during the simulation length (see Table 1).

Top BC	Ra	$\bar{\text{Nu}}_{\text{bot}}$	$\bar{\text{Nu}}_{\text{top}}$	$\bar{\text{Nu}}_\epsilon$	$\bar{\text{Nu}}_\theta$	σ_{bot}	σ_{top}
No-slip	1×10^7	13.072	13.070	13.051	13.032	1.3	1.3
	5×10^7	20.997	20.999	20.936	20.849	1.9	1.9
Free-slip	1×10^7	16.644	16.642	16.614	16.573	1.7	3.0
	5×10^7	26.975	26.974	26.885	26.695	2.5	4.4

Table 1. Time-averaged values $\bar{\text{Nu}}_{\text{bot}}$, $\bar{\text{Nu}}_{\text{top}}$ and standard deviation for the bottom and top walls Nusselt number $\sigma_{\text{bot}} = ((\text{Nu}_{\text{bot}} - \bar{\text{Nu}}_{\text{bot}})^2)^{0.5}$ and $\sigma_{\text{top}} = ((\text{Nu}_{\text{top}} - \bar{\text{Nu}}_{\text{top}})^2)^{0.5}$. Quantities evaluated using 8,000 convective time units.

3 Global angular impulse and reversals

The vorticity $\omega_c(t)$ measured at the cell centre can be used to characterize the central vortex. We define a large eddy turnover time $\tau_E = 4\pi/|\omega_c|$. The values of τ_E are $\tau_E = 4.83$ for RBC and $\tau_E = 4.46$

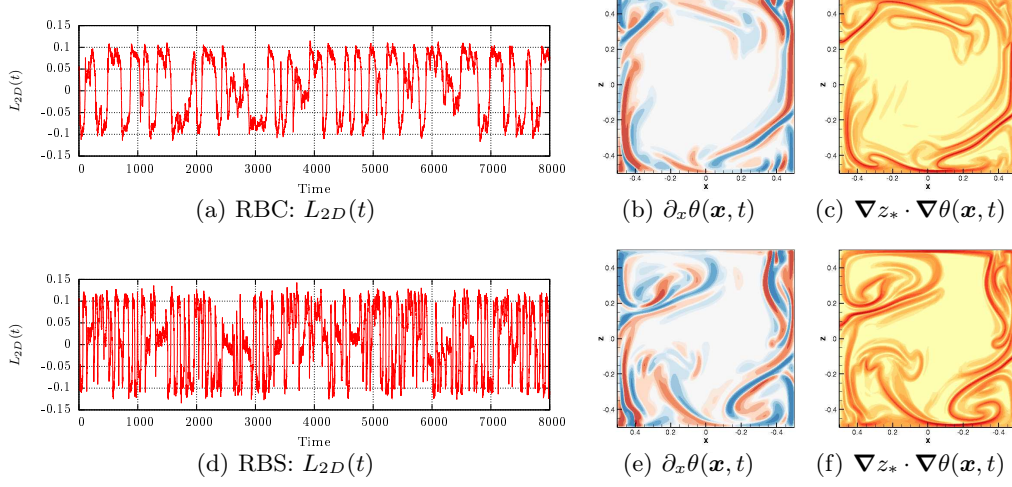


Figure 1. $Ra = 5 \times 10^7$: (a,d) Time evolution of the angular impulse with respect to the centre of the cell $L_{2D}(t) = -\frac{1}{2} \int \mathbf{x}^2 \omega(\mathbf{x}, t) d\mathbf{x}$, ω being the vorticity. (b,e) Horizontal temperature gradient $\partial_x \theta(\mathbf{x}, t)$ and (c,f) diffusive mixing term $\nabla_{z_*} \cdot \nabla \theta(\mathbf{x}, t)$.

for RBS. A better way to quantify organized rotation is to measure the global angular impulse with respect to the centre of the cell, $L_{2D} \equiv -\frac{1}{2} \int \mathbf{x}^2 \omega(\mathbf{x}, t) d\mathbf{x}$ where ω denotes the vorticity field. A flow reversal is usually defined as a rapid increase (for negative values) or decrease (for positive values) of $L_{2D}(t)$ followed by a change of sign. Figure 1 shows the evolution of $L_{2D}(t)$: flow reversals are observed in both RBC and RBS with peak values, $\max(|L_{2D}|)(t) = 0.1170$ and $\max(|L_{2D}|)(t) = 0.1068$, respectively.

In order to narrow down the definition of flow reversals, we identify points where $L_{2D}(t) = 0$, and points where a cut-off value is exceeded, $L_{2D}(t) = \pm 1/3 \max(L_{2D})$. Values of 0, +1, or -1 are assigned to these points accordingly. Looking at the sequence of these points, we are able to assign one of three possible states: *plateau* (a sequence of 1, 1, 1 or -1, -1, -1), *reversal* (a sequence of 1, 0 - 1 or -1, 0, 1), or *cessation* (every other combinations) [4]. By this procedure, we are able to provide a measure of the time spent in each state and thus to identify for each time series, the mean interval between reversals $\bar{\tau}_l$, the mean duration of a reversal $\bar{\tau}_d$.

For RBC, results are in good agreement with [3, 4] for $Ra = 5 \times 10^7$: $\bar{\tau}_l = 29.40 \tau_E = 141.3$ and $\bar{\tau}_d = 2.4 \tau_E = 15.5$. For RBS at $Ra = 5 \times 10^7$, the system spends less time in the *plateau* state ($\bar{\tau}_l = 13.3 \tau_E = 59.3$) and the reversal itself is shorter ($\bar{\tau}_d = 1.8 \tau_E = 8.1$).

Note that the global angular impulse satisfies the following equation [10]

$$\frac{dL_{2D}}{dt}(t) = \frac{\text{Pr}}{\sqrt{Ra}} \text{I} + \text{II} - \text{M} \quad (3)$$

where the I, II, and M contributions originate from diffusive terms, advective terms and external forces,

$$\begin{cases} \text{I} \equiv \oint [\omega[\mathbf{x} \cdot \mathbf{n}] - \frac{1}{2} \mathbf{x}^2 \partial_n \omega] dS - 2 \int \omega d\mathbf{x} \\ \text{II} \equiv \frac{1}{2} \oint \mathbf{u}^2 [\mathbf{n} \times \mathbf{x}] dS \\ \text{M} \equiv \frac{1}{2} \text{Pr} \int \mathbf{x}^2 \partial_x \theta d\mathbf{x} \end{cases} \quad (4)$$

For both RBS and RBC, the balance occurs between I and M, and II is negligible. For I the surface term containing $\partial_n \omega$ is larger by an order of magnitude. Note that the circulation term in I is not zero for RBS, but it plays a negligible role. Figures 1 (b) and 1 (e) show $\partial_x \theta(\mathbf{x}, t)$, which acts as the vorticity production term in the bulk and is related to M. This term is shown to be concentrated along the vertical sidewalls and at the front of colliding plumes.

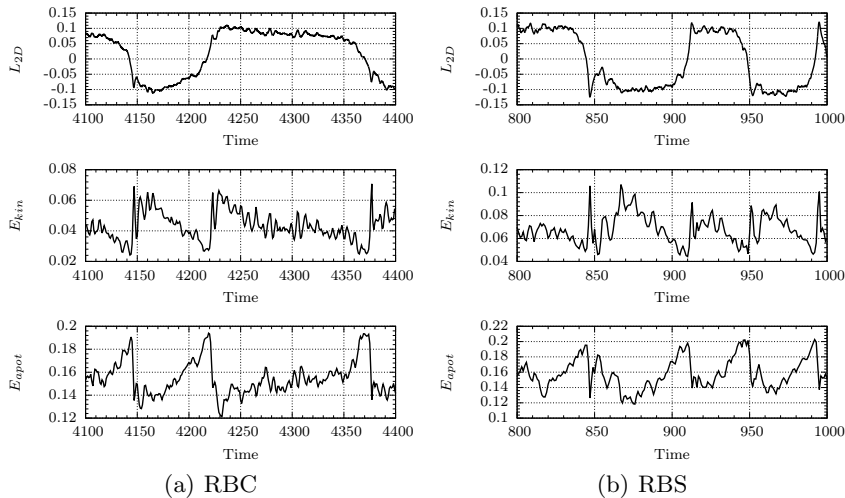


Figure 2. $Ra = 5 \times 10^7$: Time evolution for angular impulse $L_{2D}(t)$, kinetic energy $E_{kin}(t)$, and available potential energy $E_{aprot}(t)$, during consecutive reversals for (a) RBC configuration and (b) RBS configuration.

4 Mean temperature and heat flux

For the RBS cell, the mean temperature is 10% lower than $(\theta_{bot} + \theta_{top})/2$ which is the value found in RBC. A similar result was reported by [5] for free-slip side-walls and wide aspect ratio. In that case it was considered to be a flow effect heavily dependent on the initial conditions. In our case, we believe this behaviour is sustained on a long term basis because of the top/bottom BC asymmetry.

Regarding the heat flux, it increases around 40% when going from RBC to RBS configuration (see time-averaged values in Table 1). For RBC, the heat flux behaves similarly at the top and bottom walls, while for RBS the standard deviation σ_{top} almost doubles with respect to σ_{bot} (see Table 1). Note that $\sigma_{bot}/\sqrt{Nu_{bot}}$ is very close for RBS and RBC. This could lead us to think that the RBS cell behaves as a combination of one no-slip half-cell at the bottom and one free-slip half-cell at the top. A similar idea has been put forward by [11] for other asymmetric configurations.

5 Reversal mechanism: Energy build-up and release of potential energy

We study a standard reversal in terms of the mechanical energy budget. We define the global kinetic and potential energy as $E_{kin} \equiv \frac{1}{2} \langle |\mathbf{u}|^2 \rangle_V$ and $E_{pot} \equiv -\Pr \langle \theta z \rangle_V$. The potential energy itself is decomposed into available $E_{aprot} \equiv -\Pr \langle \theta(z - z_*) \rangle$ and background $E_{bpot} \equiv -\Pr \langle \theta z_* \rangle$ potential parts. Here $z_*(\mathbf{x}, t)$ denotes the height of a fluid parcel located at \mathbf{x} at time t when it is moved through virtual adiabatic motions in a reference state of minimal potential energy attainable (for more details, see Ref. [12]). At a given time t , we use the spatial probability density function of the temperature field $P(\theta)$ to obtain $z_*(\mathbf{x}, t)$ [13]:

$$z_*(\mathbf{x}, t) = z_r(\theta(\mathbf{x}, t)) \quad \text{with} \quad z_r(\theta) = \int_{-0.5}^{\theta} P(\theta) d\theta \quad (5)$$

Figure 2 displays for RBC and RBS configurations, the angular impulse, global kinetic and available potential energy during few consecutive reversals. In both cases available potential energy is building at a regular pace during the *plateau* state. It then approaches an upper bound and it is suddenly released, breaking the overall circulation. A sequence of snapshots of the temperature $\theta(\mathbf{x}, t)$ during this accumulation process is seen in Figure 3.

In this sequence, heat entering the system is transformed into available potential energy and accumulates at the counter-rotating corner flows and inside the boundary layers. Small plumes detached from

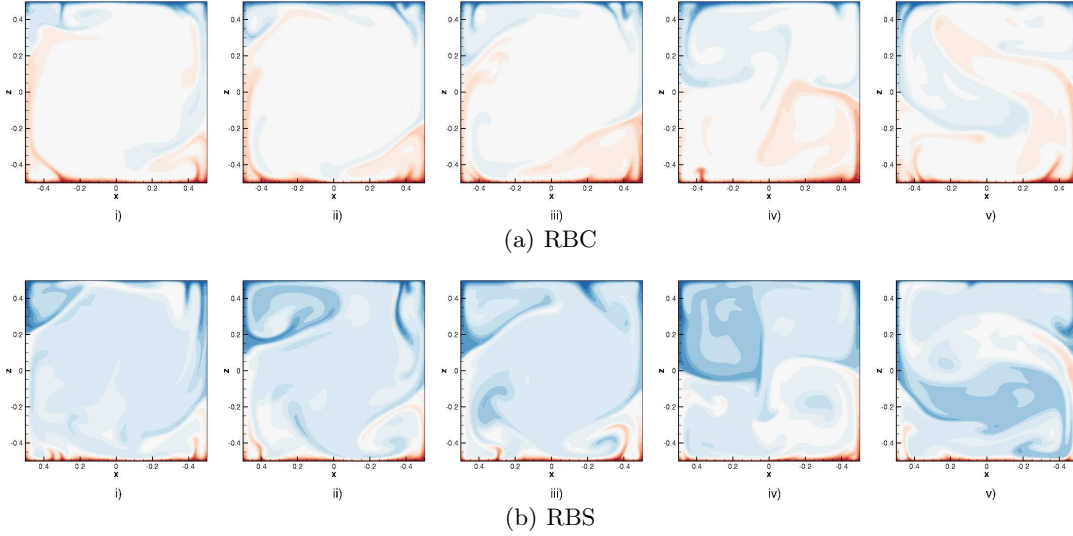


Figure 3. Evolution of temperature field at $Ra = 5 \cdot 10^7$: (a) RBC: i) $t = 4,160$, ii) $t = 4,180$, iii) $t = 4,200$, iv) $t = 4,220$, and v) $t = 4,223$; and (b) RBS: i) $t = 785$, ii) $t = 805$, iii) $t = 825$, iv) $t = 845$, and v) $t = 847$; corresponding to accumulation of energy in the corner flows up to a peak value and detachment.

the boundary layer, are dragged by the circulation and merge with larger plumes that rise/fall along the side-walls, collide with the corner flows and ultimately penetrate the opposing boundary layer, before being fed into the corner flows. Opposing corner flows grow gradually until they touch and release the energy into the bulk almost at once. The same stages are observed for both RBC and RBS, although it was observed that RBS has a significantly lower bulk temperature than RBC observed for the duration of the simulations.

Energy conversion rates between the kinetic and potential energies are given by [14]

$$\begin{cases} \frac{dE_{\text{kin}}}{dt} = \Phi_z - \epsilon & \frac{dE_{\text{pot}}}{dt} = \Phi_i + \Phi_{b1} - \Phi_z \\ \frac{dE_{\text{aprot}}}{dt} = \Phi_i - \Phi_d - \Phi_z + \Phi_{b1} + \Phi_{b2} & \frac{dE_{\text{bpot}}}{dt} = \Phi_d - \Phi_{b2} \end{cases} \quad (6)$$

$$\begin{cases} \Phi_z \equiv \text{Pr} \langle w\theta \rangle & \epsilon \equiv \text{Pr} Ra^{-\frac{1}{2}} \langle \nabla \mathbf{u} : \nabla \mathbf{u} \rangle \\ \Phi_d \equiv \text{Pr} Ra^{-\frac{1}{2}} \langle \nabla z_* \cdot \nabla \theta \rangle & \Phi_i \equiv \text{Pr} Ra^{-\frac{1}{2}} \\ \Phi_{b1} \equiv -\text{Pr} Ra^{-\frac{1}{2}} \oint z \partial_n \theta dS & \Phi_{b2} \equiv \text{Pr} Ra^{-\frac{1}{2}} \oint z_* \partial_n \theta dS \end{cases} \quad (7)$$

where Φ_z is the buoyancy flux, Φ_d the conversion rate due to irreversible mixing, and ϵ the viscous dissipation rate. Φ_{b1} and Φ_{b2} correspond to the conversion rate from heat entering the system into potential energy and background potential energy, respectively. Note that due to the imposed boundary conditions for temperature $\Phi_{b1}(t) = \Phi_{b2}(t)$, and both values are equally related to $0.5(\text{Nu}_{\text{top}} + \text{Nu}_{\text{bot}})$.

The buoyancy flux Φ_z is a measure of hot/cold ascending/descending plumes towards a thermally stable state. For both cases, this quantity peaks as the energy stored in the corners is released (Fig. 3v). It then decreases abruptly becoming negative. This seems correlated to the following observation: the deflection of plumes by the opposite walls and the return to the circulation (not shown here). The term Φ_d is always positive, mixing front is localized at the interface between the plumes and the bulk (Fig. 1(c) and (f)). This term fluctuates strongly as the circulation breaks and irreversible mixing intensifies.

In this context, the time-averaged values of Φ_z and Φ_d are not very informative since they satisfy the following relations, $\overline{\Phi_z} = \bar{\epsilon} = (\overline{\text{Nu}} - 1) \text{Pr} / \sqrt{\text{Ra}}$ and $\overline{\Phi_d} = \overline{\Phi_{b1}} = \overline{\text{Nu}} \text{Pr} / \sqrt{\text{Ra}}$ given by [14]. These equalities are verified within 1% in our simulation. Instead, we choose to show the standard deviation of these quantities during the flow reversal regime (Table 2) where a noticeable increase from RBC to RBS is observed.

Top BC	Ra	$\sigma(\Phi_z)$	$\sigma(\Phi_d)$	$\sigma(\epsilon)$	$\sigma(\Phi_{b1})$
No-slip	1×10^7	4.3	2.5	1.3	0.9
	5×10^7	7.8	4.2	2.0	1.5
Free-slip	1×10^7	8.4	4.1	2.3	1.8
	5×10^7	12.7	6.2	3.2	2.7

Table 2. Standard deviations of terms from Eq. (7), where all terms have been normalized by $\text{Pr}/\sqrt{\text{Ra}}$.

6 Conclusions

We have studied the influence of mechanical boundary conditions on Rayleigh-Bénard convection, and in particular inside the flow reversal regime. For values of $\text{Ra} = 5 \times 10^7$, $\text{Pr} = 4.3$ this flow reversal regime is observed for both no-slip and free-slip convection and is characterized by a roll-dominated convection, with a single central vortex and two-counter rotating corner flows. As the opposing corner flows grow, they touch and form a single roll, releasing the energy store into the circulation before self-organizing anew. The reversal mechanism is indeed identical for both RBC and RBS, but reversals are significantly faster and happen more frequently for RBS than RBC. For the free-slip cell the mean temperature is 10% lower than $(\theta_{\text{bot}} + \theta_{\text{top}})/2$. An increased heat-flux is also observed for free-slip convection where the Nusselt number is around 40% bigger for all values of $\text{Ra} - \text{Pr}$, consistent with previous observations [5]. We have used the angular impulse and mechanical energy budgets to provide a more complete description of the flow reversal process.

References

1. H. J. H. CLERCX, S. R. MASSEN & G. J. F. VAN HEIJST, Spontaneous spin-up during the decay of 2D turbulence in a square container with rigid boundaries, *Phys. Rev. Lett.*, **80**, 5129–5132 (1998).
2. M. CHANDRA & M. K. VERMA, Flow Reversals in turbulent convection via vortex reconnections, *Phys. Rev. Lett.*, **110**, 114503 (2013).
3. K. SUGIYAMA *et al.*, Flow reversals in thermally driven turbulence, *Phys. Rev. Lett.*, **105**, 034503 (2010).
4. B. PODVIN & A. SERGENT, A large-scale investigation of wind reversal in a square Rayleigh-Bénard cell, *J. Fluid Mech.*, **766**, 172–201 (2015).
5. E. P. VAN DER POEL, R. OSTILLA-MÓNICO, R. VERZICCO & D. LOHSE, Effect of velocity boundary conditions on the heat transfer and flow topology in two-dimensional Rayleigh-Bénard convection, *Phys. Rev. E*, **90**, 013017 (2014).
6. J. B. BELL, P. COLELLA & H. M. GLAZ, A second-order projection method for the incompressible Navier-Stokes equations, *J. Comp. Phys.*, **283**, 257–283 (1989).
7. S. POPINET, *Basilisk, an incompressible Navier-Stokes solver (centered formulation)*, <http://basilisk.fr/>.
8. R. J. A. M. STEVENS, R. VERZICCO & D. LOHSE, Radial boundary layer structure and Nusselt number in Rayleigh-Bénard convection, *J. Fluid Mech.*, **643**, 495–507 (2010).
9. B. I. SHRAIMAN & E. D. SIGGIA, Heat transport in high-Rayleigh-number convection, *Phys. Rev. A*, **42**, 3650–3653 (1990).
10. D. MOLENAAR, H. J. H. CLERCX & G. J. F. VAN HEIJST, Angular momentum of forced 2D turbulence in a square no-slip domain, *Physica D*, **196**, 329–340 (2004).
11. J. SALORT, O. LIOT *et al.*, Thermal boundary layer near roughnesses in turbulent Rayleigh-Bénard convection: Flow structure and multistability, *Phys. Fluids*, **26**, 015112 (2014).
12. K. B. WINTERS & W. R. YOUNG, Available potential energy and buoyancy variance in horizontal convection, *J. Fluid Mech.*, **629**, 221–230 (2009).
13. Y. H. TSENG & J. H. FERZIGER, Mixing and available potential energy in stratified flows, *Phys. Fluids*, **13**, 1281–1293 (2001).
14. G. HUGHES, B. GAYEN & R. W. GRIFFITHS, Available potential energy in Rayleigh-Bénard convection, *J. Fluid Mech.*, **729**, R3 (2013).